[Chem. Pharm. Bull. 25(7)1610—1635(1977)]

UDC 615.2.011.3 : 615.6.014.073

Analysis of the Stress and Strain Distributions in the Compressed Powder in the Limiting Equilibrium States Specified by the Mohr Criterion. Theory and Measurements of Mechanical Properties

Yoshinobu Fukumori[1a] and Jutaro Okada[1b]

Faculty of Pharmaceutical Sciences, Kobe Gakuin University[1a] and Faculty of Pharmaceutical Sciences, Kyoto University[1b]

(Received October 19, 1976)

The theory of the limiting equilibrium states specified by the Mohr criterion was developed for the axially symmetrical problem in regard to tabletting. The unique solution of the equilibrium equations could be obtained when the stress field and the displacement field, which was calculated by using the stress-strain relations and the displacement-strain relations, satisfied the following boundary conditions: (1) the stress on the die wall satisfies the wall yield condition and the active pressure is applied to the die wall; (2) the powder does not slide on the punches; (3) the displacement at the die wall is produced only in the direction parallel to die wall. The above relations were derived on the base of the incremental theory and the theory of the velocity field in soil mechanics.

The mechanical properties which were required for the numerical calculations on the computors were the yield locus, the wall yield locus and the stress-strain relation in the one-dimensional compression, which were obtained experimentally with the potassium chloride powder. The results of calculations showed that there appeared the region where the pressure was higher than in the neighbourhood and the region where the pressure was lower when the upper punch pressure changed from zero to 2 kg/cm^2.

Keywords——tablets; compression; powders; potassium chloride; stress-strain relations; computer application; friction; equilibrium

Introduction

The density distribution in the compressed powder becomes an important problem in tabletting, powder metallurgy, the ceramic industry, *etc.* Train[2] measured the density distribution in the compact of magnesium carbonate which was compressed from one side by upper punch. He reported that the region of lower density than that in the neighbourhood appeared in the center below the upper punch and the region of higher density appeared in the center above the lower punch. Aketa and Tsuwa[3] also obtained the similar patterns of density distribution by use of the various metal powders. It is very interesting that the similar patterns of density distribution have been obtained by use of the magnesium carbonate and metal powders which appear to differ greatly from each other in mechanical properties. However, no theoretical explanation for those patterns has been made up to the present.

In order to explain the density distribution theoretically and besides to elucidate many other problems in tabletting, *etc.*, the theory on the stress, strain and their distributions in the bed of powder must be developed.

In the analysis of static stress within the bed of powder, the theory of the limiting equilibrium states specified by the Mohr-Coulomb criterion has been used widely. On the base

1) Location: *a*) *Arise, Igawadani-machi, Tarumi-ku, Kobe*; *b*) *Yoshida-Shimoadachi-machi, Sakyo-ku, Kyoto.*
2) D. Train, *Trans. Instn Chem. Engrs*, **35**, 258 (1957).
3) Y. Aketa and H. Tsuwa, *Technol. Reports Osaka Univ.*, **18**, 489 (1968).

of this theory, the stress distribution can be calculated numerically from the equilibrium equations and the yield conditions without considering strain.[4] However, the boundary conditions of stress must be known previously. When the powder in the cylindrical die (fixed) is compressed from one side by upper punch, they can not be assumed appropriately. Clearly, they are not self-evident either. Besides it is practically difficult to measure the forces which are not distributed uniformly.

On the other hand, the boundary conditions of displacement are almost evident, because the displacements of punches can be known from the operating conditions and no displacement of the die is produced: the elastic deformation of materials of the die and punches are negligible in comparison with that of powder. Accordingly, if we can elucidate the displacement-strain relations and the stress-strain relations, the stress distribution which satisfies the boundary conditions of displacement can be determined uniquely.

In soil mechanics, the theory of velocity field[5] which is an extension of the theory of perfectly plastic solids[6] to soil medium has been used to describe the stress-strain relations in the plastic flow of soils or sands. In the case of compressed powders, all the stress-strain relations can not be given by the theory of the velocity field. That theory only relates to the shearing deformation in which the decrease in the apparent volume of powder with an increase in the isotropic component of stress can be neglected. Hence, our subject is how to introduce the decrease in the volume into the stress-strain relations.

In this paper, we develop the theory of the limiting equilibrium states specified by the Mohr criterion for the axially symmetrical problems and propose the stress-strain relations. Besides we present the methods of numerical calculations of the stress and strain distributions on the base of those theories, report the methods and the results of measurements of mechanical properties of powder required for numerical calculations, and hold the discussions on a few results of simplified calculations.

Theoretical

1. Theory of the Limiting Equilibrium States Specified by the Mohr Criterion

1.1. Equilibrium Equations——The case where the powder in the cylindrical die (fixed) is compressed from one side by a flat upper punch (the lower is also flat) is considered here. Since it is a problem of axial symmetry, it is convenient to use the cylindrical coordinates (r, θ, z), where we consider r and θ in the surface of upper punch and z, extending perpendicularly downward (that is, in the direction towards the lower punch). Let σ_r, σ_θ and σ_z be normal components of stress parallel to r-, θ- and z- axes and τ_{rz} be shearing-stress component, then the well known equilibrium equations of stress for axially symmetrical problems have the following form:[7]

$$\frac{\partial \sigma_r}{\partial r} + \frac{\partial \tau_{rz}}{\partial z} + \frac{\sigma_r - \sigma_\theta}{r} = 0$$
$$\frac{\partial \tau_{rz}}{\partial r} + \frac{\partial \sigma_z}{\partial z} + \frac{\tau_{rz}}{r} = 0 \qquad (1)$$

4) R. Aoki and M. Suzuki, *J. Chem. Eng. Japan*, **2**, 235 (1969).
5) *a*) K. Akai, "Doshitsu Rikigaku Tokuron," Morikita-Shuppan, Tokyo, 1974, p. 151; *b*) T.H. Wu, "Soil Mechanics," Allyn and Bacon, 1966, pp. 257—264.
6) W. Prager, "Rheology," Vol. 1, ed. by F.R. Eirich, Academic Press Inc. Pub., New York, 1956, p. 63.
7) *a*) S. Timoshenko and J.N. Goodier, "Theory of Elasticity," McGraw-Hill Book Co., New York, 1934, p. 343; *b*) M. Reiner, "Lectures on Theoretical Rheology," North-Holland Pub. Co., Amsterdam, 1960, pp. 26—30.

1.2. The Mohr-Coulomb Yield Condition and the Yield Surface——Let σ_Y be the normal component of stress acting on the failure surface, τ_Y be shearing-stress component, c be cohesion and δ be the angle of internal friction, then the Mohr-Coulomb yield condition is expressed by the following Eq. (2).

$$\tau_Y = c + \sigma_Y \tan\delta \tag{2}$$

Using the principal stresses σ_1, σ_2 and σ_3, we can rewrite Eq. (2) as Eqs. (3) and (4).

$$\sigma_1 = 2c\frac{\cos\delta}{1-\sin\delta} + \sigma_3\frac{1+\sin\delta}{1-\sin\delta} \qquad (\sigma_1>\sigma_2>\sigma_3) \tag{3}$$

$$\sigma_1 = 2c\frac{\cos\delta}{1-\sin\delta} + \sigma_2\frac{1+\sin\delta}{1-\sin\delta} \qquad (\sigma_1>\sigma_3>\sigma_2) \tag{4}$$

In stress space that has the rectangular Cartesian coordinates σ_1, σ_2 and σ_3, Eqs. (3) and (4) express the two planes. The directions normal to those planes are respectively as follows:

$$\left(1,\ 0,\ -\frac{1+\sin\delta}{1-\sin\delta}\right), \qquad \left(1,\ -\frac{1+\sin\delta}{1-\sin\delta},\ 0\right)$$

In the same manner, another four equations which hold in the case where σ_2 or σ_3 is the maximum principal stress can be obtained. The sides of the hexagonal pyramid in stress space which are formed by the above six planes are called 'yield surface'.[5,8]

From the axial symmetry, σ_θ must be one of the principal stresses, but it is impossible that σ_θ takes the maximum. Now, let σ_1 be the maximum principal stress. (In the following, the direction in which the principal stress σ_1 acts will be termed σ_i-direction (i=1, 2, 3)). Then, the σ_1-direction is contained by the r—z plane and the deformation in the r—z plane must be produced under the yield condition (3) or (4). In the axially symmetrical problem, the displacement in the r-direction is accompanied with the expansion or the shrinking in the θ-direction (see the third of Eqs. (32)). It is here assumed that the shearing deformation is also produced under the Mohr-Coulomb yield condition in the plane which contains the σ_1-direction and the θ-direction.

Finally, if $\sigma_\theta=\sigma_2$, the deformations in the r—z plane and the σ_1-θ plane which are perpendicular to each other are simultaneously produced under the yield conditions (3) and (4), respectively. Then, the principal stresses must satisfy the relations expressed by the intersection (5) of the two planes (3) and (4) in stress space.

$$\frac{\sigma_1-2c\dfrac{\cos\delta}{1-\sin\delta}}{\dfrac{1+\sin\delta}{1-\sin\delta}} = \sigma_2 = \sigma_3 \tag{5}$$

Hence, the following Eq. (6) hold.

$$\sigma_\theta = \sigma_2 = \sigma_3 \tag{6}$$

1.3. Expressions of σ_r, σ_θ, σ_z and τ_{rz} in Terms of the Principal Components of Stress——Since the yield conditions of powder generally become a curve in the Mohr diagram, they can not always be formulated as Eq. (2). Even in such case, c and δ in Eq. (2) can also be made constant in the narrow range of stress and therefore the discussions in Section (1.2) are acceptable. Since the overall range of stress can be divided into such narrow ranges, the above important relations (6) generally hold.

Using Eq. (6), we can express σ_r, σ_θ, σ_z and τ_{rz} in terms of the principal components of stress as follows:

8) K. Akai, "Doshitsu Rikigaku Tokuron," Morikita-Shuppan, Tokyo, 1974, p. 62.

$$\sigma_r = \frac{\sigma_1+\sigma_3}{2} - \frac{\sigma_1-\sigma_3}{2}\cos 2\varphi$$

$$\sigma_z = \frac{\sigma_1+\sigma_3}{2} + \frac{\sigma_1-\sigma_3}{2}\cos 2\varphi \qquad (7)$$

$$\tau_{rz} = \frac{\sigma_1-\sigma_3}{2}\sin 2\varphi$$

$$\sigma_\theta = \sigma_3$$

where σ_1 is the maximum, σ_3 is the minimum principal stress and φ is an angle of the z-axis to the σ_1-direction (refer to Fig. 1).

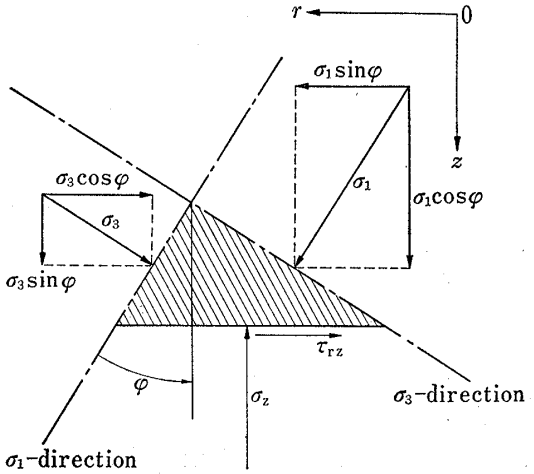

Fig. 1. Stress Acting on the Sides of Triangular Element in the r—z Plane

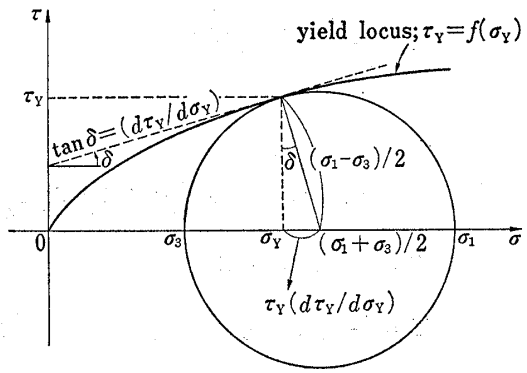

Fig. 2. Mohr Diagram

1.4. Characteristics of Equilibrium Equations——Since the yield locus of the powder compressed under high pressure can not be written generally in such a simple form as Eq. (2), we express it as follows:

$$\tau_Y = f(\sigma_Y) \equiv f \qquad (8)$$

The function f can be determined from the yield locus obtained experimentally.

It is clear from Fig. 2 that the center and the radius of a Mohr circle are given by

$$\frac{\sigma_1+\sigma_3}{2} = \sigma_Y + ff'$$

$$\frac{\sigma_1-\sigma_3}{2} = f\sqrt{1+f'^2} \qquad (9)$$

where

$$f' = \frac{df(\sigma_Y)}{d\sigma_Y}, \qquad (8')$$

namely, f' is the slope of a tangent of the yield locus. Substituting Eqs. (9) into Eqs. (7), we can rewrite Eqs. (7) in the following form:

$$\sigma_r = \sigma_Y + ff' - f\sqrt{1+f'^2}\cos 2\varphi$$

$$\sigma_z = \sigma_Y + ff' + f\sqrt{1+f'^2}\cos 2\varphi$$

$$\tau_{rz} = f\sqrt{1+f'^2}\sin 2\varphi \qquad (10)$$

$$\sigma_\theta = \sigma_Y + ff' - f\sqrt{1+f'^2}$$

Substituting Eqs. (10) into the equilibrium equations (1), we have a system (11) of hyperbolic quasi-linear partial differential equations of the first order for σ_Y and φ:

$$\begin{aligned} &A\frac{\partial\sigma_Y}{\partial r}+B\frac{\partial\sigma_Y}{\partial z}+C\frac{\partial\varphi}{\partial r}+D\frac{\partial\varphi}{\partial z}=X \\ &A'\frac{\partial\sigma_Y}{\partial r}+B'\frac{\partial\sigma_Y}{\partial z}+C'\frac{\partial\varphi}{\partial r}+D'\frac{\partial\varphi}{\partial z}=Y \end{aligned} \tag{11}$$

where

$$\begin{aligned} A &= 1+f'^2+ff'-\left(f'\sqrt{1+f'^2}+\frac{ff'f''}{\sqrt{1+f'^2}}\right)\cos 2\varphi \\ B &= \left(f'\sqrt{1+f'^2}+\frac{ff'f''}{\sqrt{1+f'^2}}\right)\sin 2\varphi \\ C &= 2f\sqrt{1+f'^2}\sin 2\varphi \\ D &= 2f\sqrt{1+f'^2}\cos 2\varphi \\ X &= -\frac{1}{r}f\sqrt{1+f'^2}(1-\cos 2\varphi) \end{aligned} \tag{12}$$

and

$$\begin{aligned} A' &= B \\ B' &= 1+f'^2+ff'+\left(f'\sqrt{1+f'^2}+\frac{ff'f''}{\sqrt{1+f'^2}}\right)\cos 2\varphi \\ C' &= D,\quad D' = -C \\ Y &= -\frac{1}{r}f\sqrt{1+f'^2}\sin 2\varphi \qquad \left(f''=\frac{d^2f(\sigma_Y)}{d\sigma_Y{}^2}\right) \end{aligned} \tag{13}$$

Following Lister,[9] we have the characteristic equations of the system (11). They are summerized in the following:

(1) Along I-slip-line,

$$\frac{dz}{dr}=\frac{\sqrt{1+f'^2}\sin 2\varphi-1}{f'-\sqrt{1+f'^2}\cos 2\varphi} \tag{14}$$

$$\frac{1+f'^2+ff''}{2f(1+f'^2)}\frac{d\sigma_Y}{dr}+\frac{d\varphi}{dr}=-\frac{\sin\varphi\{(\sqrt{1+f'^2}-f')\cos\varphi-\sin\varphi\}}{r(\sqrt{1+f'^2}\cos 2\varphi-f')} \tag{15}$$

(2) Along II-slip-line,

$$\frac{dz}{dr}=\frac{\sqrt{1+f'^2}\sin 2\varphi+1}{f'-\sqrt{1+f'^2}\cos 2\varphi} \tag{16}$$

$$\frac{1+f'^2+ff''}{2f(1+f'^2)}\frac{d\sigma_Y}{dr}-\frac{d\varphi}{dr}=\frac{\sin\varphi\{(\sqrt{1+f'^2}-f')\cos\varphi+\sin\varphi\}}{r(\sqrt{1+f'^2}\cos 2\varphi-f')} \tag{17}$$

When $r=0$, the right hand sides of Eqs. (15) and (17) can be replaced by $-d\varphi/dr$ and $d\varphi/dr$, respectively.

If we define β as follows;

$$\beta=\frac{\pi}{4}-\frac{\delta}{2}+\varphi \qquad (\delta=\tan^{-1}f')$$

(refer to Fig. 3) Eq. (14)—(17) are replaced by Eqs. (18)—(21) ($f''=0$).

(1) Along I-slip-line,

$$\frac{dz}{dr}=\cot\beta \tag{18}$$

$$\frac{1}{2f}\frac{d\sigma_Y}{dr}+\frac{d\varphi}{dr}=\frac{1}{2r}\left\{\cot\beta-\frac{\cos(\beta-2\varphi)}{\sin\beta}\right\} \tag{19}$$

9) M. Lister, "Mathematical Methods for Digital Computers," ed. by A. Ralson and H.S. Wilf, John Wiley and Sons, Inc., New York, 1960, p. 165.

(2) Along II-slip-line,

$$\frac{dz}{dr} = \cot(2\varphi-\beta) \tag{20}$$

$$\frac{1}{2f}\frac{d\sigma_Y}{dr} - \frac{d\varphi}{dr} = \frac{1}{2r}\left\{\cot(\beta-2\varphi) - \frac{\cos\beta}{\sin(\beta-2\varphi)}\right\} \tag{21}$$

It is clear that Eqs. (18) and (20) agree with the directions of slip-lines in the r—z plane.

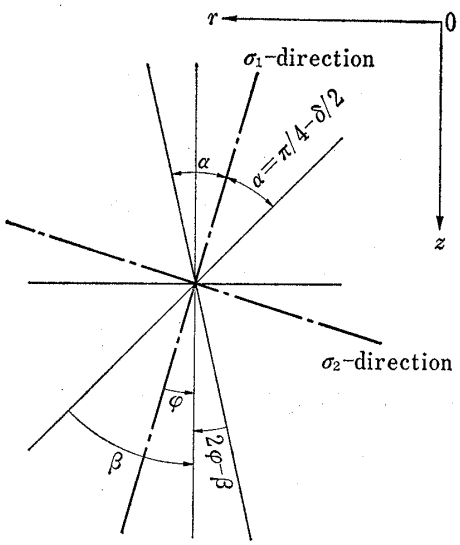

Fig. 3. Angles of the σ_1-Direction to the Slip-lines and the z-Axis

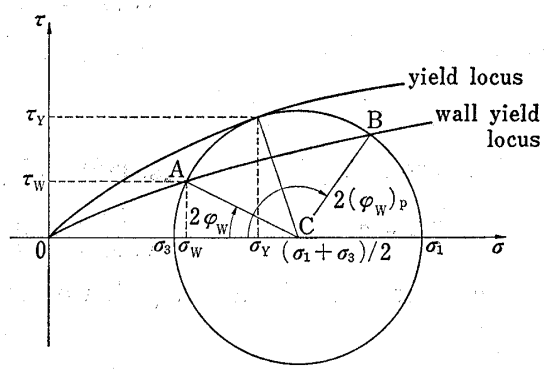

Fig. 4. Wall Yield Condition of Stress

1.5. Assumptions for the Boundary Conditions of Stress ——At first, it is assumed that the powder slides on the die wall ($r=r_W$). Then, since the stress on the die wall must satisfy the wall yield conditions, it should be represented by either A or B in Fig. 4: A and B are the intersections of a wall yield locus and a Mohr circle. Since it can be postulated that the active pressure[10] is applied to the die wall in our case, the stress on the die wall can be represented by the point A.[11] (The point B represents the stress, for example, when the bridge of powder is formed in a hopper.) Then, the angle of the die wall to σ_1-direction is φ_W (shown in Fig. 4), whose sign is always positive. Further, we also assume that the powder is in the limiting equilibrium states on the die wall. Then, φ_W become a function of σ_Y. Here we generally express φ_W as Eq. (22).

$$\varphi_W = g(\sigma_Y) \tag{22}$$

Next, on the base of the axial symmetry and Eq. (22), we shall derive the relationship equations reqired to set up the boundary conditions of stress later.

From the axial symmetry,

$$\varphi = 0 \quad \text{at } r = 0 \tag{23}$$

Hence, on the symmetrical axis, the coefficients (12) of the first of equilibrium equations (11) reduce to

$$A_a = (1+f'^2+ff'')\left(1-\frac{f'}{\sqrt{1+f'^2}}\right), \quad B_a = C_a = 0, \quad D_a = 2f\sqrt{1+f'^2},$$

10) *a*) D.W. Taylor, "Fundamentals of Soil Mechanics," John Wiley and Sons, Inc., New York, 1948, p. 422; *b*) J.K. Walters, *Chem. Eng. Sci.*, **28**, 13 (1973).

11) As will be shown in Fig. 29, $\mu_W K$ in Janssen's equation takes the value 0.1—0.24. Measured values of μ_W are about 0.3—0.5 (Fig. 20—22). If the active pressure is applied to the die wall, K can be approximated by σ_3/σ_1 whose value is 0.3—0.4 (Fig. 15). Hence, $\mu_W K$ should take the value 0.09—0.2, which agrees well with the above value 0.1—0.24. If the passive pressure is applied to the die wall, $\mu_W K$ must take the value 1.7—0.75: in this case, K can be approximated by σ_1/σ_3. Hence, it can be postulated that the passive pressure is not applied to the die wall and hence the bridge of powder is not formed.

$$X_a = \lim_{\substack{\varphi\to 0\\ r\to 0}} \left\{-\frac{1}{r}\sqrt{1+f'^2}(1-\cos 2\varphi)\right\} = 0$$

Accordingly, the first of Eqs. (11) reduces to

$$A_a\left(\frac{\partial \sigma_Y}{\partial r}\right)_a + D_a\left(\frac{\partial \varphi}{\partial z}\right)_a = 0 \qquad \text{at } r = 0 \tag{24}$$

where A_a is the value of A taken on the symmetrical axis and so on. Since $(\partial\varphi/\partial z)_a=0$ (clear from Eq. (23)), finally Eq. (24) reduces to

$$\frac{\partial \sigma_Y}{\partial r} = 0 \qquad \text{at } r = 0 \qquad \left(\left(\frac{\partial \sigma_Y}{\partial r}\right)_a = 0\right) \tag{25}$$

Further, differentiating the second of Eqs. (10) with respect to r, we have

$$\frac{\partial \sigma_z}{\partial r} = B'\frac{\partial \sigma_Y}{\partial r} - C\frac{\partial \varphi}{\partial r} \tag{26}$$

which reduces to Eq. (27) from Eqs. (23) and (25).

$$\frac{\partial \sigma_z}{\partial r} = 0 \qquad \text{at } r = 0 \qquad \left(\left(\frac{\partial \sigma_z}{\partial r}\right)_a = 0\right) \tag{27}$$

On the other hand, from Eq. (22), we have the following expression (28) which hold on the die wall.

$$\left(\frac{\partial \varphi}{\partial z}\right)_W = \frac{\partial \varphi_W}{\partial \sigma_Y}\left(\frac{\partial \sigma_Y}{\partial z}\right)_W = g'\left(\frac{\partial \sigma_Y}{\partial z}\right)_W \tag{28}$$

where the suffix W means that the values of derivatives are taken on the die wall. Substituting Eq. (28) into Eq. (11), then we have

$$E\left(\frac{\partial \sigma_Y}{\partial r}\right)_W + F\left(\frac{\partial \varphi}{\partial r}\right)_W = G \tag{29}$$

where

$$E = A_W(B'_W + D'_W g') - A'_W(B_W + D_W g')$$
$$F = C_W(B'_W + D'_W g') - C'_W(B_W + D_W g')$$
$$G = X_W(B'_W + D'_W g') - Y_W(B_W + D_W g')$$

Eliminating $(\partial \sigma_Y/\partial r)_W$ from Eqs. (26) and (29), we have

$$E\left(\frac{\partial \sigma_z}{\partial r}\right)_W = B'_W G - (B'_W F + C_W)\left(\frac{\partial \varphi}{\partial r}\right)_W \tag{30}$$

The above Eqs. (23), (27) and (30) are of great importance in the analysis of the stress distribution in the case where there is no singular point on the boundary. The details will be found later (see Section (3.1)).

It is possible that the points $(r_W, 0)$ and (r_W, h), which are the intersections of the die wall and the planes of upper and lower punches, become singular (h is the thickness of the bed of powder). While only two sliplines can be drawn in the r—z plane through any point except for singular points, an infinite number of slip-lines can be drawn through a singular point.[12]

Now, for convenience, we rewrite Eq. (15) as Eq. (15′) to derive the equilibrium equation which should hold at the singular point $(r_W, 0)$.

$$\frac{1}{2f'}d\left\{\ln\left(f\sqrt{1+f'^2}\right)\right\} + d\varphi = -\frac{\sin\varphi\{(\sqrt{1+f'^2}-f')\cos\varphi - \sin\varphi\}}{r(\sqrt{1+f'^2}\cos 2\varphi - f')}dr \tag{15′}$$

Let the intersections of II-slip-lines ($\varphi=\varphi_1$, φ_2, $\cdots$ and φ_n) drawn through the singular point A $(r_W, 0)$ and a I-slip-line drawn in the neighbourhood of A be B_1, B_2, $\cdots$ and B_n as shown in Fig. 5. When the I-slip-line is gradually brought closer to the point A, the value

12) V.A. Florin, "Florin no Doshitsu Rikigaku," trans. by S. Ogusa, Morikita-Shuppan, Tokyo, 1971, Vol. 3, p. 24.

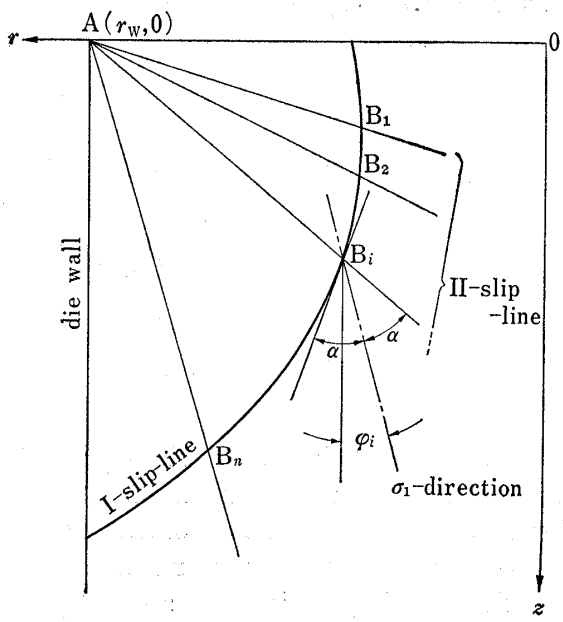

Fig. 5. Slip-lines Drawn through the Singular Point

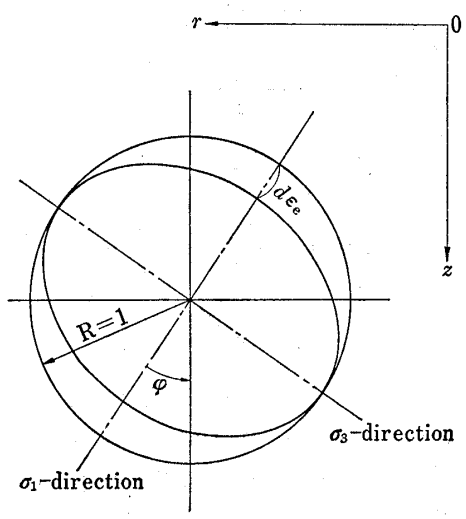

Fig. 6. Transformation of the Circle with a Radius of Unity to the Ellipse ('Strain Ellipese') by Strainin the σ_1-Direction

of $d\varphi=\varphi_{i+1}-\varphi_i$ (φ_i and φ_{i+1} correspond to the points B_i and B_{i+1}, respectively) remains finite, while the value of $dr=r_{i+1}-r_i$ in Eq. (15′) becomes unlimitedly small. Hence, Eq. (31) must hold at the singular point A.

$$\frac{1}{2f'}d\left\{\ln\left(f\sqrt{1+f'^2}\right)\right\}+d\varphi=0 \qquad (31)$$

If the value of σ_Y corresponding to the II-slip-line $\varphi=\varphi_1$ is known, the values of σ_Y coresponding to the other II-slip-lines can be calculated numerically by the finite-difference method according to Eq. (31).

The fundamental equations for the analysis of stress in the compressed powder have been developed so far. If the boundary conditions of stress are known, the stress distribution should be determined according to these equations. But, in our case, the conditions of stress on the upper punch can not be known.

2. The Incremental Theory and the Stress-strain Relations

Since the deformation of powder in the compression under high pressure such as tablet formation is large, the theory of infinitesimal strain used in the classical theory of elasticity can not be applied to our problem as it is. There are two kinds of theories on large deformation, which are the incremental theory[13] and the finite deformation theory.[14] We shall apply the incremental theory to the analysis of strain in the bed of powder.

In the compression of powder in the cylindrical die, the thickness of the bed of powder can change from the initial thickness h_0 to h_m which is the thickness of the bed containing no void. This process of compaction is divided into many small steps. Then, for each step, the theory of infinitesimal strain can be developed.

For the axially symmetrical deformation, the component of displacement in the θ-direction vanishes. The components of the increment of displacement in the r- and z-directions are denoted by du_r and du_z, respectively. Since we can make the increment of strain very small or infinitesimal according to the incremental theory, the increment of strain (taken

13) Y. Yamada, "Matrix-ho no Oyo," ed. by Y. Yamada, Tokyo Univ. Shuppan-kai, Tokyo, 1972, p. 149.
14) R.S. Rivlin, "Rheology," ed. by F.R. Eirich, Academic Press Inc. Pub., New York, Vol. 1, 1956, p. 354.

positive when it produces compression) can be expressed by Eqs. (32) as components in the directions of coordinate axes.[7b]

$$d\varepsilon_r = -\frac{\partial du_r}{\partial r}$$

$$d\varepsilon_z = -\frac{\partial du_z}{\partial z}$$

$$d\varepsilon_\theta = -\frac{du_r}{r} \tag{32}$$

$$d\varepsilon_{rz} = -\frac{\partial du_r}{\partial z} - \frac{\partial du_z}{\partial r}$$

$$d\varepsilon_{\theta z} = d\varepsilon_{r\theta} = 0$$

As has been described in Introduction and was discussed in our previous paper,[15] we must introduce the decrease in the apparent volume of powder induced by the isotropic component of stress into the stress-strain relations. Clearly we can not obtain the dense compacts without such a property of powder. Further, since powders must be compressed in the shape determined by the die and punches, the shearing strain must also be produced in the bed of powder. However, it is impossible without the decrease in the apparent volume, because shearing is restricted by the die wall and the punches whose materials are greatly rigid on comparing with powder. Further the increase in the apparent volume accompanies the shearing of powder.[5,16] Hence the total change in the apparent volume can be given approximately by the summation of the above two.

Since it is inconvenient to measure the decrease in the apparent volume induced by the isotropic component of stress directly,[15] we introduce it in the following manner:

2.1. Compression in the σ_1-Direction when no Strain is produced in the σ_2- and σ_3-Directions (One-dimensional Compression)——Since the frictional force acts on the die wall in the case of compression of the powder in a die, the stress and strain distributions within the bed of powder are not uniform. However, as was described in our previous paper,[15] we can cancel the frictional force by extrapolating the amount of powder filled into the die to zero. Then, we can consider the bed of powder to be in the following state: the stress and strain are uniform; the maximum principal stress σ_1 acts in the direction of symmetrical axis; no strain is produced in the radius direction. In the following, we shall derive the stress-strain relations for the powder compressed under the above conditions. Clearly, the decrease in the apparent volume induced by the isotropic component of stress is included by those stress-strain relations.

Let h_e be the thickness of the cylindrical bed of powder. Further, we define the dimensionless thickness $\bar{h}$ as follows:

$$\bar{h} = \frac{h_e}{h_{e,0}} = \bar{h}(\sigma_1) \tag{33}$$

where $h_{e,0}$ is the value of h_e when $\sigma_1=0$. The increment $d\varepsilon_e$ of strain induced by the change of σ_1^A to σ_1^B is defined by

$$d\varepsilon_e = \frac{h_e^A - h_e^B}{h_e^A} = \frac{\bar{h}(\sigma_1^A) - \bar{h}(\sigma_1^B)}{\bar{h}(\sigma_1^A)} \tag{34}$$

$d\varepsilon_e$ is the instantaneous strain proposed by Hencky.[17]

15) J. Okada and Y. Fukumori, *Yakugaku Zasshi*, **94**, 285 (1974).
16) *a*) D.W. Taylor, "Fundamentals of Soil Mechanics," John Wiley and Sons, Inc., New York, 1948, p. 335; *b*) S.C. Cowin, *Powder Technology*, **9**, 61 (1974); *c*) P.W. Rowe, *Geotechnique*, **19**, 1 (1969).
17) *a*) M. Reiner, "Lectures on Theoretical Rheology," North-Holland Pub. Co., Amsterdam, 1960, p. 12; *b*) H. Hencky, *Ann. Physik*, **2**, 617 (1929).

Fig. 6 shows the strain ellipse[18] corresponding to one-dimensional compression. The strain $d\varepsilon_e$ in the σ_1-direction is produced in the r—z plane: zero in the σ_3- and θ-directions. Then the components of strain in the directions of coordinate axes are expressed as follows:[18]

$$\begin{aligned} d\varepsilon_{r,1} &= \frac{d\varepsilon_e}{2}(1-\cos 2\varphi) \\ d\varepsilon_{z,1} &= \frac{d\varepsilon_e}{2}(1+\cos 2\varphi) \\ d\varepsilon_{rz,1} &= d\varepsilon_e \sin 2\varphi \\ d\varepsilon_{\theta,1} &= 0 \end{aligned} \tag{35}$$

where $d\varepsilon_{r,1}$, $d\varepsilon_{\theta,1}$ and $d\varepsilon_{z,1}$ are compressive strains in the directions of r-, θ- and z-axes, respectively, and $d\varepsilon_{rz,1}$ is shearing strain. Eq. (35) can be derived easily in accordance with the formula of linear transformation of coordinates.

2.2. Shearing in the r—z Plane under Mohr's Yield Conditions——In this section, we shall derive the strain produced by shearing in the r—z plane under Mohr's yield conditions, following the theory of velocity field in soil mechanics.[5]

The yield function Q is defined by Eq. (36).

$$Q = (\sigma_r+\sigma_z)\sin\delta - \sqrt{(\sigma_r-\sigma_z)^2+4\tau_{rz}^2} = -2c\cos\varphi \tag{36}$$

Eq. (36) is an expression of the yield surface (3) by the components of stress in the directions of coordinate axes. From Eq. (36), the components of the increment of strain in the r- and z-directions can be expressed as follows:

$$\begin{aligned} d\varepsilon_{r,2} &= -\lambda_2\frac{\partial Q}{\partial\sigma_r} = -(\sin\delta+\cos 2\varphi)\lambda_2 \\ d\varepsilon_{z,2} &= -\lambda_2\frac{\partial Q}{\partial\sigma_z} = -(\sin\delta-\cos 2\varphi)\lambda_2 \\ d\varepsilon_{rz,2} &= -\lambda_2\frac{\partial Q}{\partial\tau_{rz}} = 2\sin 2\varphi\cdot\lambda_2 \end{aligned} \tag{37}$$

where λ_2 is a parameter.

2.3. Strain induced by the Displacement in the r-Direction——It is assumed that the increment of strain in the θ-direction induced by the displacement in the r-direction is produced by the same kind of shearing as that described in section (2.2). However, in this case, the shearing is produced in the plane which contains the θ- and σ_1-directions. Hence, we can obtain Eq. (38) as the components of the increment of strain in the θ- and σ_1-directions. (Let λ_3 be the parameter in this case.)

$$\begin{aligned} d\varepsilon_{\theta,3} &= -(\sin\delta+1)\lambda_3 \\ d\varepsilon_{1,3} &= -(\sin\delta-1)\lambda_3 \end{aligned} \tag{38}$$

It is also assumed that the component of the increment of strain in the σ_3-direction contained by the r—z plane is zero. Hence, the components in the r- and z-directions can be expressed as follows:

$$\begin{aligned} d\varepsilon_{r,3} &= \frac{1-\sin\delta}{2}(1-\cos 2\varphi)\lambda_3 \\ d\varepsilon_{z,3} &= \frac{1-\sin\delta}{2}(1+\cos 2\varphi)\lambda_3 \\ d\varepsilon_{rz,3} &= (1-\sin\delta)\sin 2\varphi\cdot\lambda_3 \end{aligned} \tag{39}$$

2.4. The Total Increments of Strain——The matrix of linear transformation of the circle to the ellipse shown in Fig. 6 can be expressed as follows:

18) J.C. Jaeger, "Elasticity, Fracture and Flow," John Wiley and Sons, Inc., New York, 1956.

$$\begin{pmatrix} 1-d\varepsilon_{r,1} & -d\varepsilon_{rz,1} \\ -d\varepsilon_{rz,1} & 1-d\varepsilon_{z,1} \end{pmatrix}$$

For the deformations described in sections (2.2) and (2.3), the same expressions can also be obtained (Replace the suffix '1' by '2' or '3'). The matrix of the transformation to the final strain ellipse can be given by the product of those three matrices. Since we can make the increment of strain very small or infinitesimal, the resultant matrix can be expressed as follows:

$$\begin{pmatrix} 1-\sum_{i=1}^{3} d\varepsilon_{r,i} & -\sum_{i=1}^{3} d\varepsilon_{rz,i} \\ -\sum_{i=1}^{3} d\varepsilon_{rz,i} & 1-\sum_{i=1}^{3} d\varepsilon_{z,i} \end{pmatrix}$$

Hence, from Eqs. (35), (37), (38) and (39), the total increment of strain is given by Eq. (40) as components.

$$\begin{aligned} d\varepsilon_r &= -\frac{\partial du_r}{\partial r} = \frac{d\varepsilon_e}{2}(1-\cos 2\varphi(+)-\sin\delta-\cos 2\varphi)\lambda_2 \\ &\quad + \frac{1-\sin\delta}{2}(1-\cos 2\varphi)\lambda_3 \\ d\varepsilon_z &= -\frac{\partial du_z}{\partial z} = \frac{d\varepsilon_e}{2}(1+\cos 2\varphi) + (-\sin\delta+\cos 2\varphi)\lambda_2 \\ &\quad + \frac{1-\sin\delta}{2}(1+\cos 2\varphi)\lambda_3 \\ d\varepsilon_\theta &= -\frac{du_r}{r} = -(1+\sin\delta)\lambda_3 \\ d\varepsilon_{rz} &= -\frac{\partial du_z}{\partial r} - \frac{\partial du_r}{dz} = d\varepsilon_e \sin 2\varphi + 2\lambda_2 \sin 2\varphi + (1-\sin\delta)\lambda_3 \sin 2\varphi \end{aligned} \tag{40}$$

where $d\varepsilon_e$ and δ are generally functions of σ_Y. Eq. (40) are the stress-strain relations expressed as increments.

3. Methods of Numerical Calculations

The flow chart to outline problems is shown in Fig. 7.

3.1. Setting of the Boundary Conditions of Stress on the Upper Punch——At first, we divide the mean pressure on the upper punch into equal small steps in stead of the total change of the thickness (h_0-h_m), though the necessity of the incremental theory is due to the large deformation. But, it does not come into question, if the increment dP_U of the pressure on the upper punch is sufficiently small.

Since the conditions of stress on the upper punch are not known, we express them by the following polynomials:

$$\sigma_z = \sum_{i=1}^{m} a_i \left(\frac{r}{r_w}\right)^{i-1}, \quad \varphi = \sum_{i=1}^{n} b_i \left(\frac{r}{r_w}\right)^{i-1} \tag{41}$$

The mean value of σ_z on the upper punch must agree with a given value of P_U. That is,

$$P_U = \frac{\int_0^{r_w} 2\pi r \sigma_z dr}{\int_0^{r_w} 2\pi r dr}$$

Hence, from the first of Eq. (41), a_1 can be expressed as Eq. (42).

$$a_1 = P_U - 2\sum_{i=2}^{m} \frac{a_i}{i+1} \tag{42}$$

Besides, since the derivative of σ_z in respect with r can be expressed from the first of Eqs. (41) as follows;

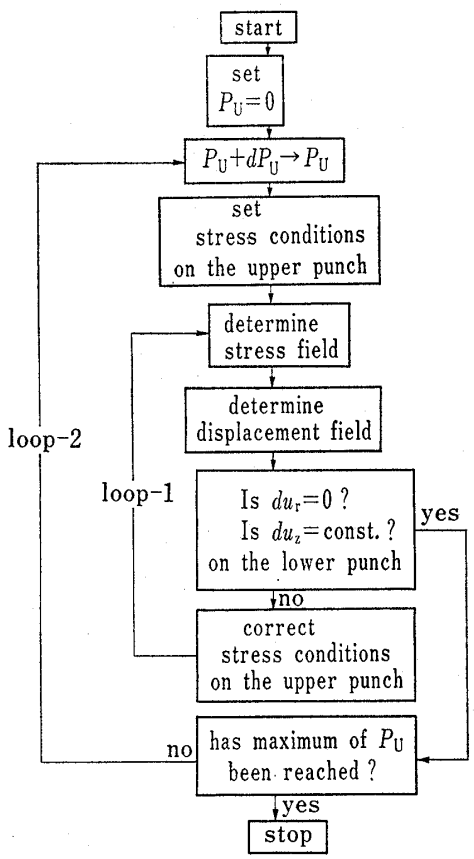

Fig. 7. Simplified Flow Chart

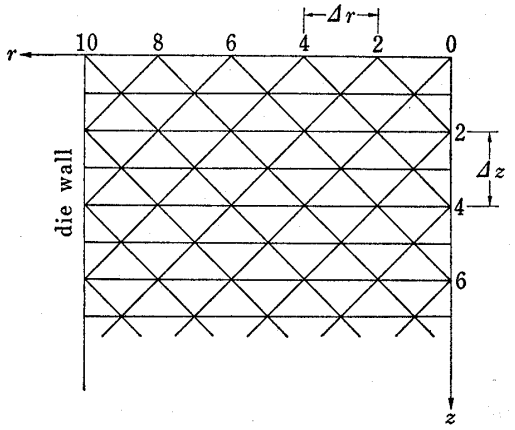

Fig. 8. Nets in the r—z Plane

$$\frac{\partial \sigma_z}{\partial r}=\sum_{i=2}^{m}\frac{(i-1)a_i r^{i-2}}{r_W{}^{i-1}} \tag{43}$$

Eq. (44) can be obtained from Eq. (27).

$$a_2=0 \tag{44}$$

In regard to φ, from Eq. (23),

$$b_1=0 \tag{45}$$

Next, we shall consider the conditions of stress at the point $(r_W, 0)$.

3.1.1. When $(r_W, 0)$ Does not become a Singular Point: From Eqs. (44) and (43),

$$\left(\frac{\partial \sigma_z}{\partial r}\right)_W=\frac{1}{r_W}\sum_{i=3}^{m}(i-1)a_i \tag{46}$$

Substituting Eq. (46) into Eq. (30), we have

$$\left(\frac{\partial \varphi}{\partial r}\right)_W=\frac{B'_W G-\frac{E}{r_W}\sum_{i=3}^{m}(i-1)a_i}{B'_W F+C_W} \tag{47}$$

From Eqs. (47) and the derivative of the second of Eqs. (41) in respect with r, b_3 is given by

$$b_3=\frac{r_W B'_W G-E\sum_{i=3}^{m}(i-1)a_i}{2(B'_W F+C_W)}-\frac{b_2}{2}-\frac{1}{2}\sum_{i=4}^{n}(i-1)b_i \tag{48}$$

Since $\varphi=\varphi_W$ at $(r_W, 0)$, from the second of Eqs. (41) we have

$$b_2=\varphi_W-\sum_{i=3}^{n}b_i \tag{49}$$

Finally, there are five relationship equations (42), (44), (45), (48) and (49) among $m+n$ numbers of constants in Eqs. (41).

The order of calculations is practically as follows: (1) a_1 can be calculated from the given values of a_i ($i=3, \cdots m$) and P_U in accordance with Eq. (42).

(2) σ_z can then be calculated at any point on the upper punch from the first of Eq. (41).

(3) $(\sigma_Y)_W$ can be calculated, when the value of $(\sigma_z)_W$ obtained above and Eqs. (8), (8′) and (22) are substituted into the second of Eq. (10) and then it is solved for σ_Y. (($)_W$ means a value taken on the die wall.)

(4) φ_W can be calculated, when $(\sigma_Y)_W$ is substituted into Eq. (22).

(5) The values of E, F, G, B'_W and C_W in Eq. (48) can then be calculated by using $(\sigma_Y)_W$ and φ_W obtained above.

(6) Substituting φ_W and the given values of b_i ($i=4, \cdots n$) into Eq. (49), Eq. (48) and (49) become a simultaneous equation for b_2 and b_3. Solving the simultaneous equation, b_2 and b_3 can be obtained easily.

(7) φ at any point on the upper punch can then be calculated from the second of Eq. (41).

(8) σ_Y, which is required to solve Eqs. (14)—(17) or (18)—(21), can be calculated from the second of Eq. (10).

3.1.2. When (r_W, 0) becomes a Singular Point: In this case, b_2 and b_3 can be given arbitrarily. Hence, the relationship equations among the constants in Eq. (41) reduce to only three equations (42), (44) and (45). The values of σ_Y and φ at (r_W, 0) calculated from Eq. (41) are identical to the values of $\sigma_{Y,1}$ and φ_1 in the limit when B_1 approaches A (refer to Fig. 5 and section (1.5)). Hence, φ_1 must satisfy the following inequality (50) in the limit.

$$-(\varphi_W)_p \leqq \varphi_1 < \varphi_W \tag{50}$$

where $(\varphi_W)_p$ is the angle shown in Fig. 4. When $\varphi_1 = -(\varphi_W)_p$ in the limit, the passive pressure[10] is applied to the upper punch at (r_W, 0). Clearly, φ_n at B_n shown in Fig. 5 is equal to φ_W in the limit.

3.2. Calculations of the Stress Distribution——Solving Eqs. (14)—(17) or (18)—(21) under the boundary conditions by the finite-difference methods numerically, we can obtain the stress distribution. Since the details of the finite-difference methods have been described by Lister,[9] they are omitted here.

3.3. Calculations of the Distribution of Displacement——The r-z plane is divided into small finite elements after the manner of the finite element method.[13] Then, on the base of the assumption that in each element the strain is uniform, the displacement at any point in the element can be calculated in accordance with Wqs. (40). An example of nets is shown in Fig. 8, where $r_W=10$, $\Delta r=\Delta z=2$. In practice, we calculated by use of the net where $\Delta r=\Delta z=0.5$.

The outline of calculations will be described below.

When the known stress field $\boldsymbol{P}$ changes to the unknown stress field $\boldsymbol{P}^*$, the increment $d\boldsymbol{U}$ of displacement field which is induced in the bed of powder must be calculated. (Points, coordinates, *etc.*, after deformation will be shown by the suffix* below.) The calculation of $d\boldsymbol{U}$ results in the calculation of the increment $d\boldsymbol{u}^P$ of displacement produced at the point P (shown in Fig. 9) when the coordinates of the nodes A, B and P before deformation (namely, when the stress field is $\boldsymbol{P}$) and the increments of displacements at the nodes A and B are known. If $d\boldsymbol{u}^P$ can be calculated, the increment of displacement at every node can be calculated stepwise from the boundary conditions which are known previously.

In regard to boundary conditions, it can be assumed that no displacement is produced on the surface of upper punch:

$$du_r = du_z = 0 \qquad \text{on the upper punch} \tag{51}$$

which corresponds to the fact that the powder does not slide on the surface of upper punch. (du_r and du_z are the components of displacement $d\boldsymbol{u}$ in the r- and z-directions, respectively.) For the same reason, the boundary conditions (52) must be satisfied by the displacement of

every node on the lower punch:

$$du_r = 0, \quad du_z = \text{const.} \qquad \text{on the lower punch} \tag{52}$$

Further, the displacement at any point on the die wall must satisfy the following boundary condition (53). Besides, it is clear from the axial symmetry that Eq. (53) also hold on the symmetrical axis.

$$du_r = 0 \qquad \text{on the die wall or on the } z\text{-axis} \tag{53}$$

Eqs. (51)—(53) are based on the facts that the origin of coordinates is fixed to the surface of upper punch and the elastic deformation of material of the die and punches is negligible on comparing with that of powder. Hence, in Eq. (52), the displacement of lower punch is relatively produced in spite of the compression from one side by upper punch.

After all, the increments of displacements of nodes on the surface of lower punch are produced by $d\boldsymbol{P}=\boldsymbol{P}^*-\boldsymbol{P}$, and $d\boldsymbol{P}$ must be determined so as to satisfy the boundary conditions (51)—(53). If described in a concrete form, the arbitrary constants in Eqs. (41) must be determined so as to minimize the sum of square of deviation from the boundary conditions (52).

The method of calculation of the displacement of node will be described below.

3.3.1. Points which are neither on the Symmetrical Axis nor on the Die Wall: It is assumed that the strain is uniform within the triangle ABP with the apices A, B and P (shown in Fig. 9). Hence, the distribution of the increment of displacement can be written in the following matrix form:

$$\begin{pmatrix} du_r \\ du_z \end{pmatrix} = \begin{pmatrix} du_r^{\mathrm{A}} \\ du_z^{\mathrm{A}} \end{pmatrix} + \begin{pmatrix} t_1 & t_3-\omega \\ t_3+\omega & t_2 \end{pmatrix} \begin{pmatrix} r-r^{\mathrm{A}} \\ z-z^{\mathrm{A}} \end{pmatrix} \tag{54}$$

Substituting the coordinates and the increment of displacement of the point B into Eq. (54), we have

$$t_1 = \frac{du_r^{\mathrm{B}} - du_r^{\mathrm{A}}}{\Delta r} \tag{55}$$

$$t_3+\omega = \frac{du_z^{\mathrm{B}} - du_z^{\mathrm{A}}}{\Delta r} \tag{56}$$

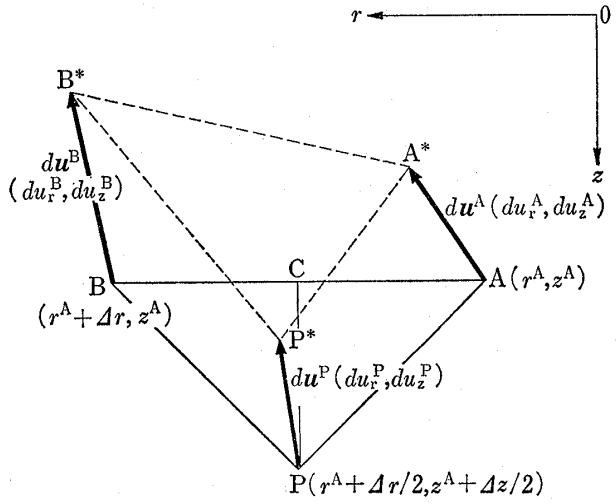

Fig. 9. Triangular Element when the Point P is neither on the Symmetrical Axis nor on the Die Wall

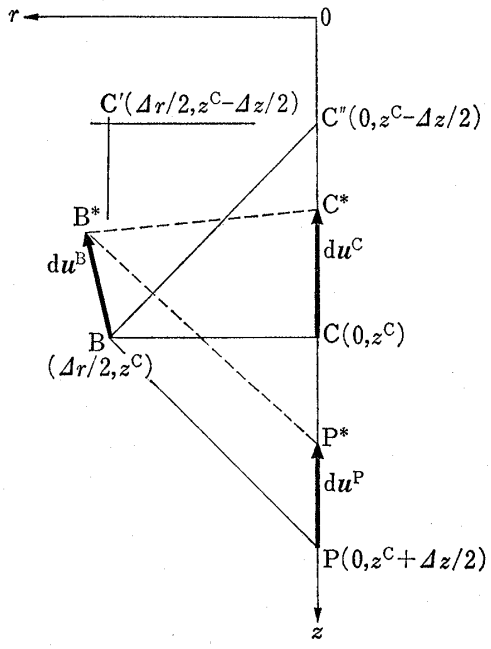

Fig. 10. Triangular Element when P is on the Symmetrical Axis

From the first of Eq. (40) and Eq. (54),

$$t_1 = \frac{\partial du_r}{\partial r} = -d\varepsilon_r = -\frac{d\varepsilon_e}{2}(1-\cos 2\varphi) + (\sin\delta+\cos 2\varphi)\lambda_2 - \frac{1-\sin\delta}{2}(1-\cos 2\varphi)\lambda_3$$

Hence, λ_2 can be calculated in accordance with the following Eq. (57).

$$\lambda_2 = \frac{t_1+\frac{d\varepsilon_e}{2}(1-\cos 2\varphi)+\frac{1-\sin\delta}{2}(1-\cos 2\varphi)\lambda_3}{\sin\delta+\cos 2\varphi} \tag{57}$$

where λ_3 is given by Eq. (58). (refer to the third of Eq. (40))

$$\lambda_3 = \frac{1}{2(1+\sin\delta)}\left(\frac{du_r{}^A}{r^A}+\frac{du_r{}^B}{r^A+\Delta r}\right) \tag{58}$$

which is the average of the values of λ_3 at the points A and B. It is assumed that λ_2 and λ_3 are also constant in the element ABP.

From the second of Eq. (40) and Eq. (54),

$$t_2 = \frac{\partial du_z}{\partial z} = -d\varepsilon_z = -\frac{d\varepsilon_e}{2}(1+\cos 2\varphi) + (\sin\delta-\cos 2\varphi)\lambda_2 - \frac{1-\sin\delta}{2}(1+\cos 2\varphi)\lambda_3 \tag{59}$$

It is clear that t_3 in Eq. (54) corresponds to half the shearing-strain component. That is, from Eq. (54),

$$\frac{\partial du_z}{\partial r}+\frac{\partial du_r}{\partial z} = t_3+\omega+t_3-\omega = 2t_3$$

Hence, from the fourth of Eq. (40),

$$t_3 = -\frac{1}{2}\{d\varepsilon_e+2\lambda_2+(1-\sin\delta)\lambda_3\}\sin 2\varphi \tag{60}$$

Substituting the value of t_3 obtained from Eq. (60) into Eq. (56), we can calculate ω corresponding to the rotation of rigid body.

Now, all the constants in Eq. (54) have been calculated. When we substitute the coordinates of the point P into Eq. (54), the required $d\boldsymbol{u}^P$ can be obtained. However, the values of φ,δ and $d\varepsilon_e$ are required for the calculations. For φ and δ, a suitable mean value in the stress fields $\boldsymbol{P}$ and $\boldsymbol{P}^*$ may be used. For example, the average of six values at the points A, B and P in the stress field $\boldsymbol{P}$ and A*, B* and P* in $\boldsymbol{P}^*$ can be used. However, since the coordinates of P* is not known previously, we give them a suitable initial value (for example, the value at A*) and make the displacement of P converge to a constant value. $d\varepsilon_e$ can be given the mean value of $d\varepsilon_e{}^A$, $d\varepsilon_e{}^B$ and $d\varepsilon_e{}^P$. For example, $d\varepsilon_e{}^A$ is calculated in accordance with the following equation:

$$d\varepsilon_e{}^A = \frac{\bar{h}(\sigma_1{}^A)-\bar{h}(\sigma_1{}^{A*})}{\bar{h}(\sigma_1{}^A)}$$

3.3.2. Points on the Synnnetrical Axis: The triangular element BCP in this case is shown in Fig. 10. We must previously calculate the displacement of C′, which is not a node, by an interpolation method and then calculate the displacement of C by applying the method described in this section.

Since the element is adjacent to the symmetrical axis, it can be assumed that the shearing-stress component and the rotation ω are zero. Besides $du_r{}^C$ and r^C are also zero. Hence, the distribution of the increment of displacement can be given by

$$\begin{pmatrix} du_r \\ du_z \end{pmatrix} = \begin{pmatrix} 0 \\ du_z{}^C \end{pmatrix} + \begin{pmatrix} t_1 & 0 \\ 0 & t_2 \end{pmatrix}\begin{pmatrix} r \\ z-z^C \end{pmatrix} \tag{61}$$

Substituting the coordinates of the point B into Eq. (61), we have

$$t_1 = \frac{du_r{}^B}{r^B} \tag{62}$$

Since $\varphi=0$, from Eq. (57) we have

$$\lambda_2 = \frac{t_1}{1+\sin\delta} \tag{63}$$

In regard to λ_3, when $r=0$, we have

$$d\varepsilon_\theta = \lim_{r\to 0}\left(-\frac{du_r}{r}\right) = -\frac{\partial du_r}{\partial r} = d\varepsilon_r$$

Hence, substituting $\varphi=0$ into the first and the third of Eq. (40), we have the following expressions:

$$d\varepsilon_r = -(\sin\delta+1)\lambda_2$$
$$d\varepsilon_\theta = -(\sin\delta+1)\lambda_3$$

Hence,

$$\lambda_3 = \lambda_2 \tag{64}$$

Substituting $\varphi=0$ and Eq. (64) into Eq. (59), we have Eq. (65).

$$t_2 = -d\varepsilon_e + 2(\sin\delta-1)\lambda_2 \tag{65}$$

3.3.3. Points on the Die Wall: The element ACP in this case is shown in Fig. 11. Since $du_r=0$ on the die wall, we have

$$\begin{pmatrix} du_r \\ du_z \end{pmatrix}\begin{pmatrix} 0 \\ du_z{}^C \end{pmatrix} + \begin{pmatrix} t_1 & t_3-\omega \\ t_3+\omega & t_2 \end{pmatrix}\begin{pmatrix} r-r^C \\ z-z^C \end{pmatrix}, \tag{66}$$

$$t_1 = -\frac{du_r{}^A}{\Delta r} \tag{67}$$

and

$$\lambda_3 = 0 \tag{68}$$

Substituting $du_r{}^P=0$ and the coordinates of the point P into Eq. (66), we have

$$du_r{}^P = (t_3-\omega)(z^P-z^C) = 0$$

Hence,

$$\omega = t_3 \tag{69}$$

Finally, the distribution of the increment of displacement reduces to

$$\begin{pmatrix} du_r \\ du_z \end{pmatrix} = \begin{pmatrix} 0 \\ du_z{}^C \end{pmatrix} + \begin{pmatrix} t_1 & 0 \\ 2t_3 & t_2 \end{pmatrix}\begin{pmatrix} r-r^C \\ z-z^C \end{pmatrix} \tag{70}$$

3.4. Correction of the Conditions of Stress on the Surface of Upper Punch——Such $d\boldsymbol{P}$ as to minimize the sum of square of deviation from the boundary conditions (52) can be given by the loop-1 shown in Fig. 7. In our methods of calculations, $d\boldsymbol{P}$ is determined by the increments $da_i=a_i{}^*-a_i$ and $db_j=b_j{}^*-b_j$ of the constants in Eqs. (41). The methods of correction of the boundary conditions of stress on the upper punch will be described below in the case where $(r_W, 0)$ is not a singular point.

The number of constants to which arbitrary values can be given is $n_f=m+n-5$. Hence, we select n_f numbers of nodes on the lower punch and let the components of the increments of displacements of those nodes in the r- and z-directions be $du_{r,k}$ and $du_{z,k}$ $(k=1,2,\cdots, n_f)$. Then, the square of deviation from the boundary conditions (52) at each node can be expressed as follows:

$$S_k = (\overline{du}_z - du_{z,k})^2 + (du_{r,k})^2 \tag{71}$$

where

$$\overline{du}_z = \frac{\sum_{k=1}^{n_f} du_{z,k}}{n_f}$$

Next, the simultaneous equation (72) for Δa_i and Δb_j is solved.

$$\sum_{i=s}^{m}\left(\frac{\partial S_k}{\partial a_i}\right)\Delta a_i + \sum_{j=t}^{n}\left(\frac{\partial S_k}{\partial b_j}\right)\Delta b_j = -S_k \qquad (72)$$

Since $\partial S_k/\partial a_i$, *etc.*, in Eq. (72) can not be calculated analytically, numerical calculations must be carried out. After Δa_i and Δb_j have been obtained, the calculations on the loop-1 is repeated by using the new values $a_i^* + \Delta a_i$ and $b_j^* + \Delta b_j$. In such manner, a_i^* and b_f^* which minimize $\sum_{k=1}^{n_f} S_k$ may be obtained.

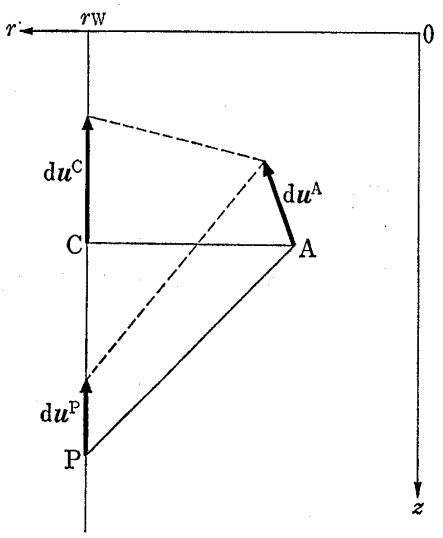

Fig. 11. Triangular Element when P is on the Die Wall

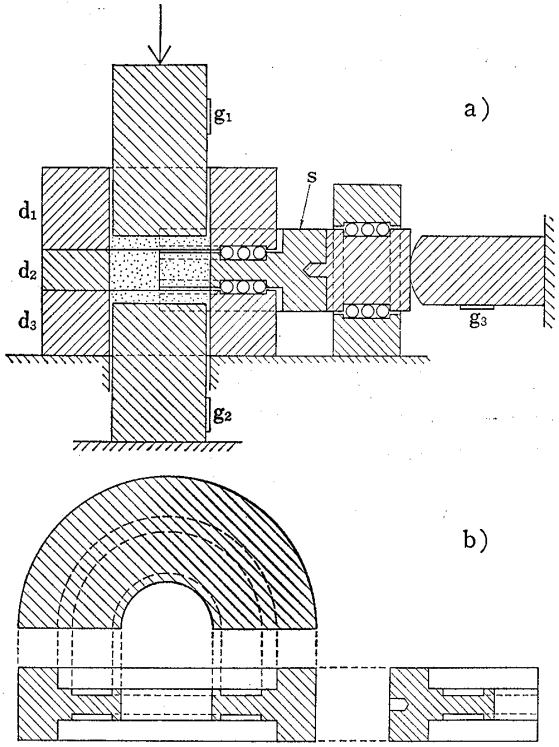

Fig. 12. Scheme of the Apparatus for the Measurement of Die Wall Pressure

Experimental

1. **Sample**——The powder of cristalline potassium chloride, 42—65 mesh, was used as a sample. The powder was prepared in the same manner as had been described in the previous paper.[19]

2. **Measurements of the Yield Locus of Powder**——Fig. 12-a is the scheme of the apparatus for measuring lateral pressure. The die with an inside diameter of 20.45 mm is divided into the three layers: d_1; d_2; d_3. Fig. 12-b shows the right half of d_2 in the magnified scale. The strain gauges g_1, g_2 and g_3 were used to measure the forces. The surfaces of die and punches contacting directly with powder were coated with an alcohlic solution of Na-stearate and then dried to decrease the frictional force. The powder, 3.5913 g, was filled into the die so that the bed was 5.5 mm thick at zero porosity.

The maximum principal stress σ_1 produced within the bed of powder was calculated in accordance with Eq. (73):[20]

$$\sigma_1 = P_L + \frac{(P_U - P_L)h_c}{h} \qquad (73)$$

where P_U and P_L are the upper and the lower punch pressures, respectively, h_c is the height of the center of d_2 to the flat surface of lower punch and h is the thickness of the bed of powder. The thickness h was measured by use of the differential transformer. The minimum principal stress was calculated from the amount of force detected by the strain gauge g_3. Then, the loss of force due to the friction of guides was neglected.

19) J. Okada and Y. Fukumori, *Chem. Pharm. Bull.* (Tokyo), 22, 493 (1974).
20) Since the value of P_L/P_U, 0.9, was fairly large, a sufficient degree of approximation can be obtained by Eq. (73).

A Mohr circle can be described in the Mohr diagram from one pair of the measured values of σ_1 and σ_3. The envelope of all the Mohr circles is the yield locus of powder. In practice, we determined a yield point in the following manner:

Let the point of contact between the Mohr circle M_i and the straight line which is tangent to the two circles M_i and M_{i+j} be $A_{i,j}$: the suffix i is the number given to the Mohr circles (obtained experimentally) in the order of size. We regarded the middle point of $A_{i,-1}$and $A_{i,+1}$ as the yield point on the Mohr circle M_i.

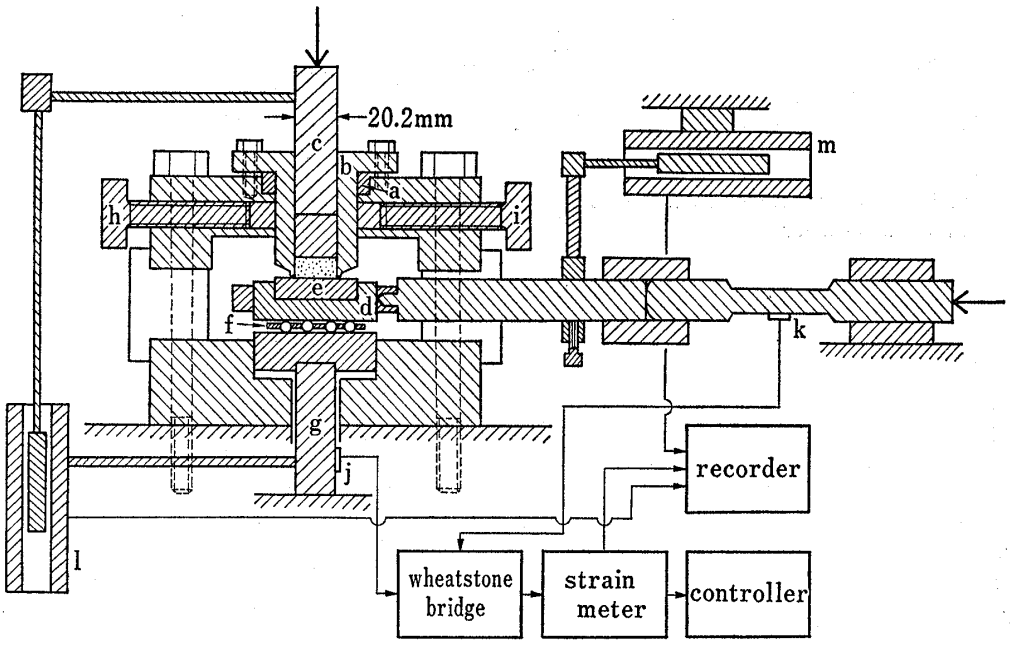

Fig. 13. Scheme of Apparatus for the Measurement of the Coefficients of Wall Friction

3. Measurements of the Coefficient of Wall Friction——Fig. 13 is the scheme of the apparatus for measuring the coefficient of wall friction. The powder, 2 g, was filled into the die b with an inside diameter of 20.20 mm. The frictional force between the powder and the circular plate e of stainless steel was measured by means of the strain gauge k. The plate e is held by the slider d. A space to be adjusted to 0.1—0.2 mm by the ring a was left between the upper surface of the plate e and the end of die b. The loss of force due to the friction in rolling of balls f was found negligible. The force normal to the sliding surface was measured by use of the strain gauge j. The normal force was kept nearly constant by means of the controller during the sliding of slider d. The displacements of the slider d and the upper punch c were measured by use of the differential transformers m and l, respectively. The die b, the upper punch c and the sliding plate e were boiled in the solution of about 5% potassium hydroxide in the 1: 1 mixture of alcohl and water, washed with distilled water and dried in the stream of dried air before measurements. Three kinds of sliding plates, whose surfaces were polished with the sand cloths of 180, 400 and 600 meshes, were used for measurements.

When the tangential pressure acting on the sliding surface is plotted to the normal in the Mohr diagram, we can obtain the wall yield locus.

4. Measurements of the P_U-e (porosity) Relations——Compressions were carried out from one side by the upper punch. The cylindrical die of an inside diameter of 20.11 mm were used. The rate of displacement of upper punch was 0.046 mm/sec, which was adjusted to the velocity of sliding in the measurements of wall friction as well as possible.

Result and Discussion

The experimental data required for the numerical calculations are the Mohr yield locus (8), the wall yield locus and the h- σ_1 relation (33). The results of measurements of those mechanical properties and the simplified calculations will be described below.

1. The Mohr Yield Locus

Fig. 14 and 15 shows the results obtained by the compression at the constant rate of displacement of upper punch, 0.046 mm/sec.

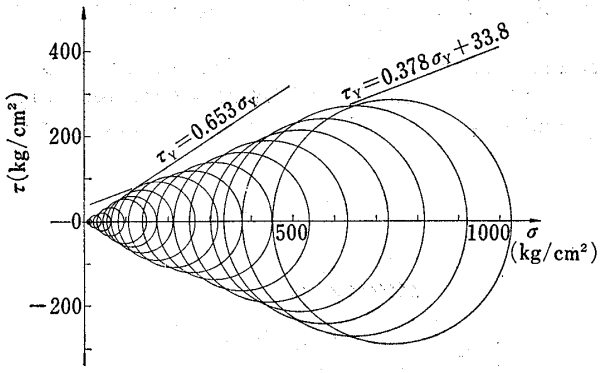

Fig. 14. Mohr Circles of the Potassium Chloride Powder

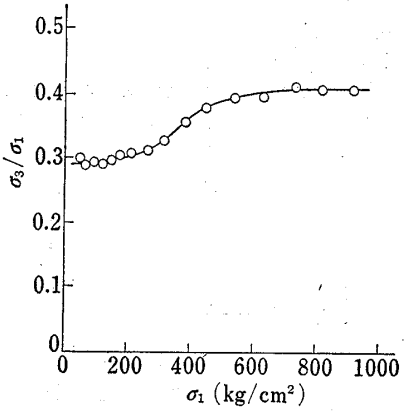

Fig. 15. Plots of σ_3/σ_1 to σ_1

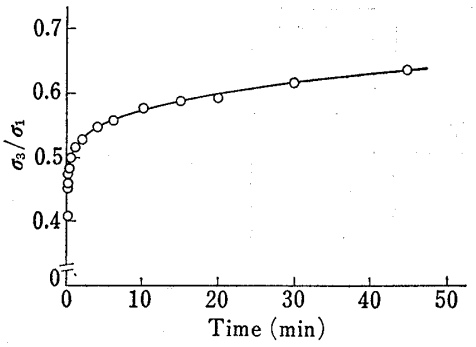

Fig. 16. Increase of σ_3/σ_1 with Time

P_U was kept constant, 1039 kg/cm², continuously after the compression at the constant rate of displacement of upper punch, 0.046 mm/sec.

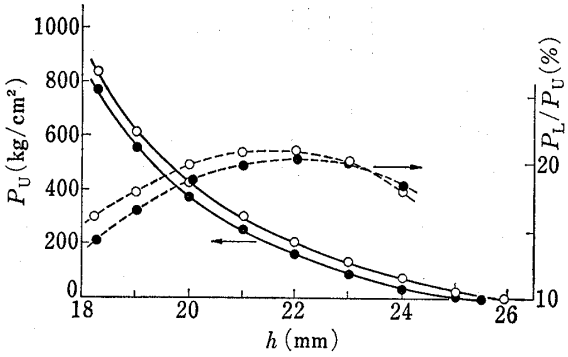

Fig. 17. Influence of the Rate of Displacement of Upper Punch on the Relation between the Upper Punch Pressure and the Thickness of Powder Bed and P_L/P_U (Pressure-transmission-ratio)

Rate of displacement of upper punch (mm/sec): ○, 0.825; ●, 0.0742.
Inside diameter of die (mm): 8.02.
Weight of powder (g): 1.5.
Die wall was cleaned in the same manner as in Section 3 in Experimental.

Measured Mohr circles are shown in Fig. 14. The yield locus can be approximated partially by the straight lines shown in Fig. 14.

Fig. 15 shows the relation between the ratio σ_3/σ_1 of principal stresses and σ_1. The relation has a tendency similar to the results reported in the previous paper.[15] However, the values themselves of σ_3/σ_1 are fairly smaller. The mechanical property of potassium chloride powder such as shown in Fig. 16 contributes to the disagreement between the above two results. Fig. 16 shows that σ_3/σ_1 increases with time at the constant upper punch pressure of 1039 kg/cm² and the increase continues even after 45 miniutes. Since the powder was compressed at the constant pressure for 10 minutes in the previous investigation, σ_3/σ_1 could take the large values there.

Clearly, the increase in σ_3/σ_1 can bring about a decrease in the pressure-transmission-ratio P_L/P_U. Fig. 17 shows effects of the rate of displacement of upper punch on P_L/P_U and the thickness-pressure relations. As may be expected from Fig. 16, the ratio P_L/P_U takes larger values at the high velocity than at the low one.

2. The Coefficient of Wall Friction

Fig. 18 shows some examples of records of the coefficient μ_W of wall friction. The upper and lower lines shows μ_W and the displacement of slider, respectively. Both the displace-

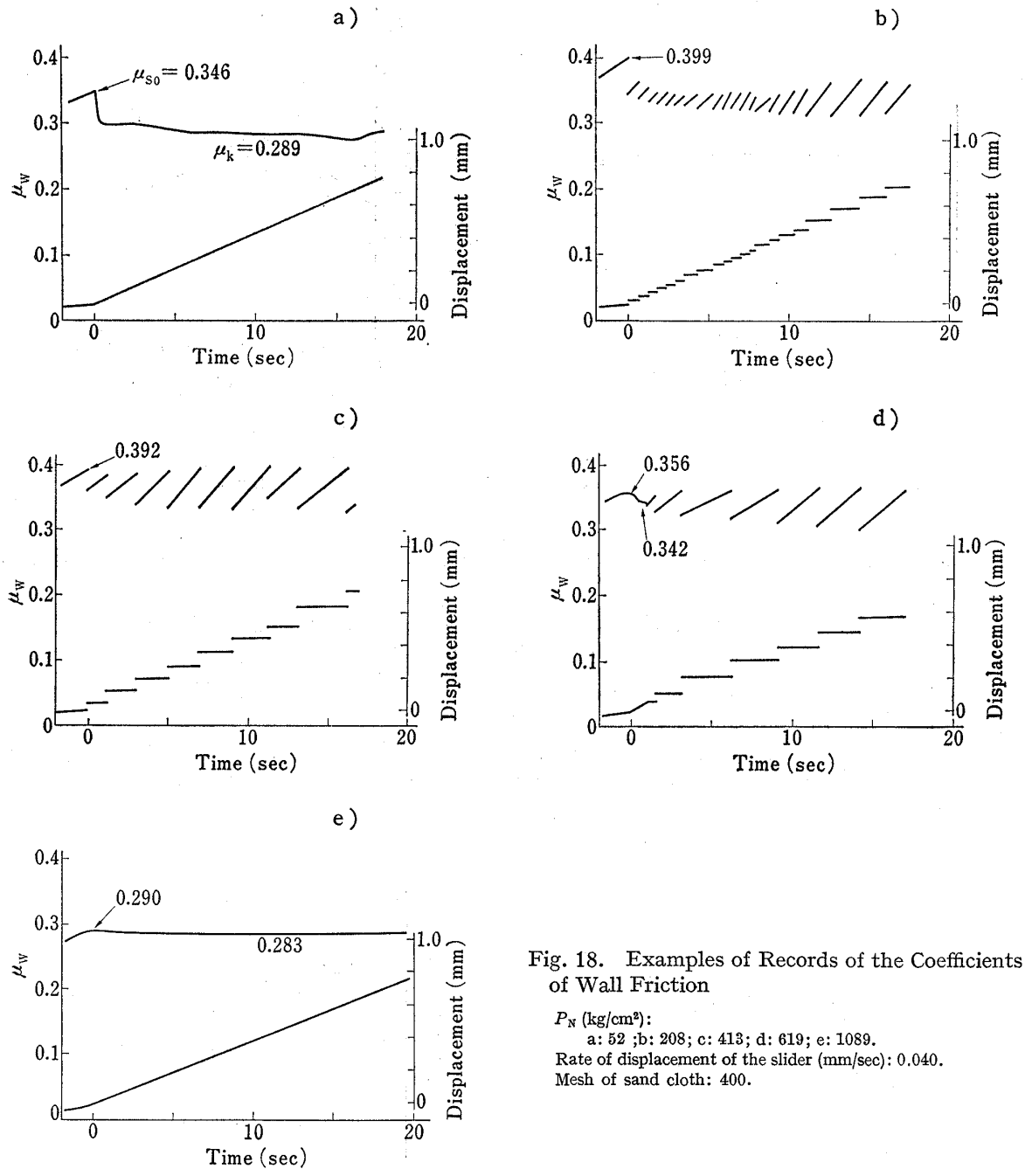

Fig. 18. Examples of Records of the Coefficients of Wall Friction

P_N (kg/cm²):
a: 52 ;b: 208; c: 413; d: 619; e: 1089.
Rate of displacement of the slider (mm/sec): 0.040.
Mesh of sand cloth: 400.

ment and time are zero when the sliding begins. In Fig. 18, P_N is normal pressure, μ_k is the coefficient of kinetic friction and μ_{s0} is the coefficient of static friction, μ_s, when the time is zero.

The smoth sliding is produced when P_N=52 and 1089 kg/cm² (Fig. 18–a, e). When P_N=208, 413 and 619 (Fig. 18. b–d), the phenomenon called 'stick-slip' occurrs:[21] the resting stage and the rapid slip appear by turns as can be found from the displacement-time relations.

Fig. 19 is the scheme of the stick-slip'. Bowden and Tabor[21] indicated that in Fig. 19 the point A corresponds to μ_s and the mean value of $\mu_W{}^A$ and $\mu_W{}^B$, which are the values of μ_W at A and B respectively, corresponds to μ_k. When P_N=619, the value of μ_k in the 'stick-slip' obtained by following Bowden and Tabor is 0.336. This value agrees well with

21) F.P. Bowden and D. Tabor, "The Friction and Lubrication of Solids," Clarendon Press, Oxford, 1954.

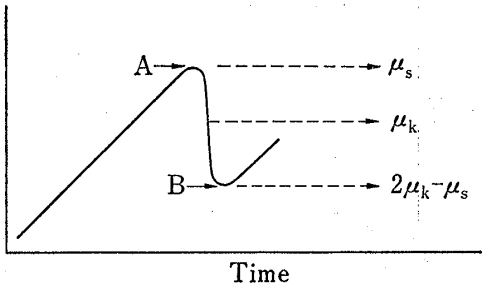

Fig. 19. 'Stick-slip'

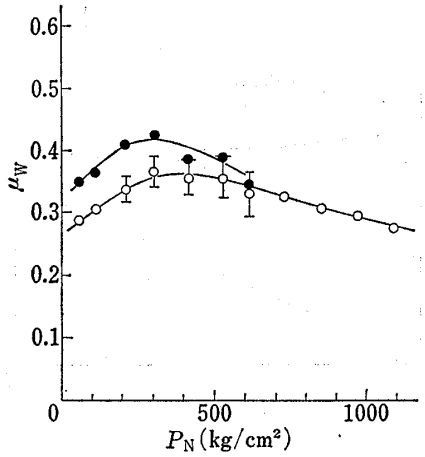

Fig. 20. Plots of μ_W to P_N
Mesh of sand cloth: 400.
○, μ_k; ●, μ_{s0}.

the value, 0.342, in the kinetic friction which appears tempotarily at the beginning of sliding (Fig. 18-d).

In Fig. 20, μ_k and μ_{s0} are plotted to P_N. When P_N is lower than 100—200, the smooth sliding occurrs. When P_N is in the range of about 200—600, the 'stick-slip' appears and then μ_k takes the large value equal to about 0.35. In this range, the amplitudes of vibration in the 'stick-slip' are shown in Fig. 20. In the range of pressure lower than about 600, μ_s takes larger values than μ_k, though it has been observed in various cases. When P_N is larger than about 600—700, the smooth sliding occurrs again and μ_k decreases gradually with the increase in P_N.

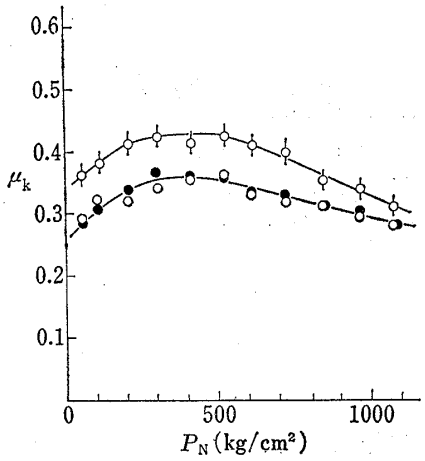

Fig. 21. Influence of the Roughness of the Surface of the Sliding Plate on μ_k
Mesh of sand cloth:
○, 600; ●, 400; ○, 180.

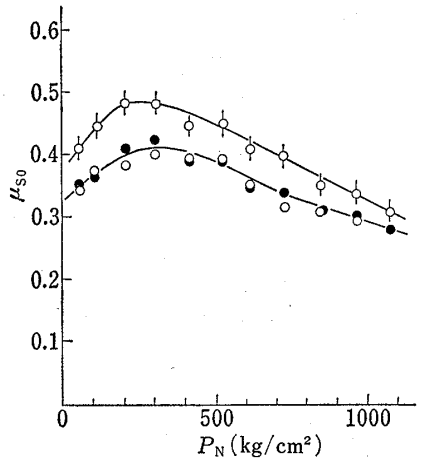

Fig. 22. Effects of the Roughness of the Surface of the Sliding Plate on μ_{s0}
Mesh of sand cloth:
○, 600; ●, 400; ○, 180.

Fig. 21 and 22 show the effects of the roughness of the surface of sliding plate on μ_k and μ_{so}, respectively. Although μ_W in the case of 400 mesh takes almost the same values as μ_W in the case of 600 mesh, μ_W in the case of 180 mesh is larger over all the range than in the other cases.

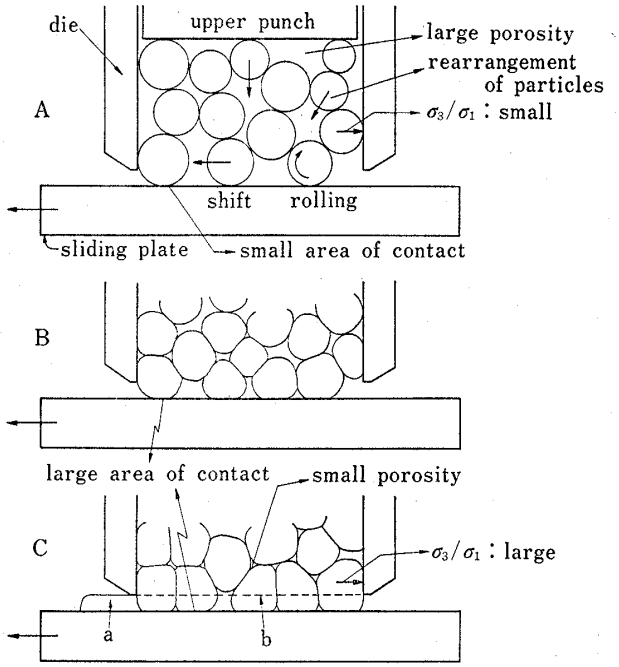

Fig. 23. Schematic Diagram of the Process of Wall Friction

	P_N (kg/cm²)	
A	<100—200	smooth sliding
B	200—600	stick-slip
C	>600—700	smooth sliding

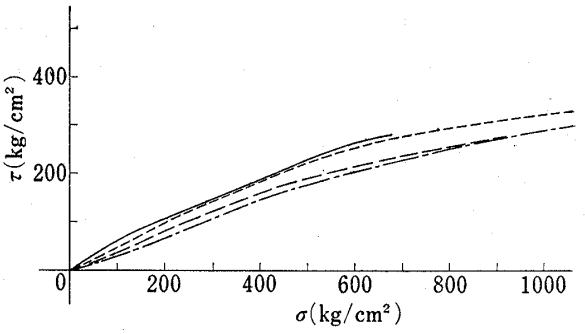

Fig. 24. Yield Locus and Wall Yield Loci of Potassium Chloride Powder

Mesh of sand cloth:
———: 400 (μ_k); ———: 400 (μ_{s0}); - - - - -: 180 (μ_{s0}).
———: yield locus of powder.

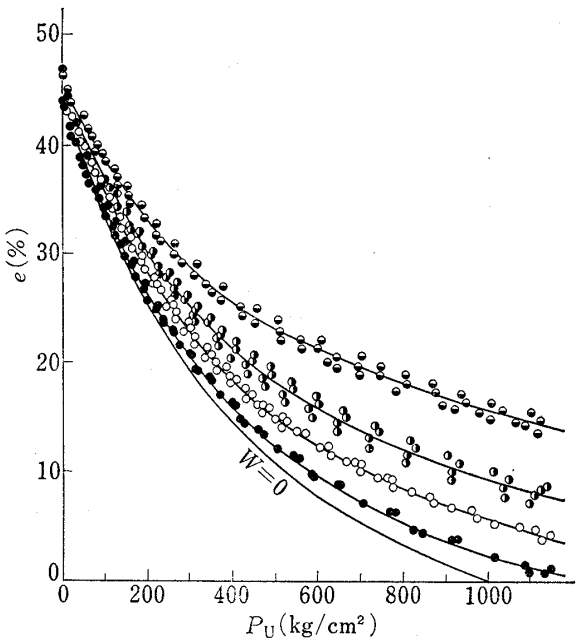

Fig. 25. Pressure-porosity Relations of Potassium Chloride Powder

Weight of powder (g):
●, 3.918; ○, 7.835; ◑, 15.671; ◒, 23.506.
$\overline{W=0}$: extrapolated to zero weight (see Fig. 26).
Inside diameter of die (mm): 20.11.

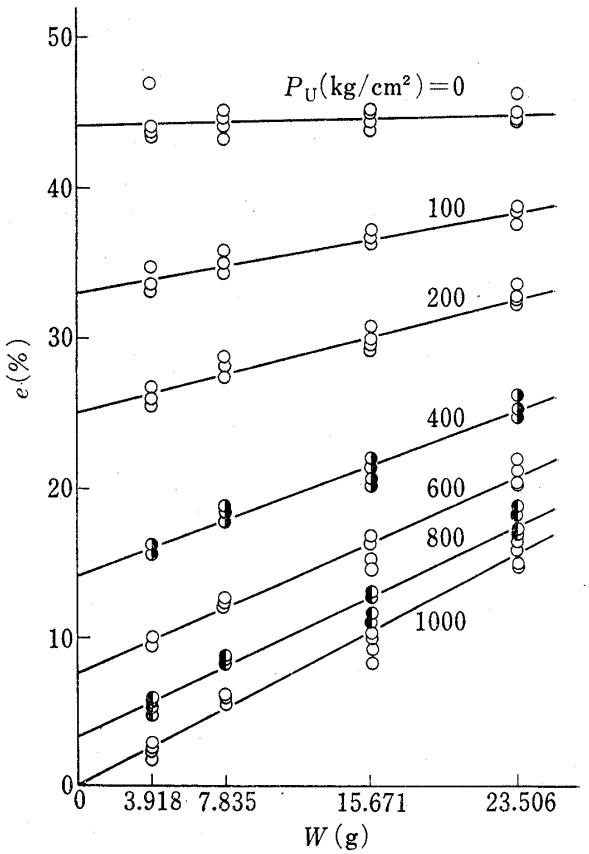

Fig. 26. Relations between e and W under the Constant Upper Punch Pressure

Fig. 23 is the scheme of the process of wall friction. (As regards the deformation of potassium chloride particle, refer to our previous paper[19]). In A, the large decrease in the apparent volume was observed during the sliding: especially large at the beginning of sliding. This is due to the large porosity of the bed of powder (Fig. 25). In such a loose packing structure, the rolling of particle must be possible. In B, the area of contact between particle and particle, or particle and metal plate, is large.[19] Hence, the shift and rolling of particle must be impossible. In C, potassium chloride was extruded as thin layer (shown by a). This suggests that the material can slip on the surface within particles, as shown by b. The sliding on the surface of metal plate should also occur in C, since μ_W is affected by the roughness of surface of sliding plate (Fig. 21 and 22). Besides, the results shown in Fig. 15 means that σ_3/σ_1 in A is smaller than that in B or C.

The yield locus of powder and the wall yield loci are together shown in Fig. 24.

3. The $\bar{h}$- σ_1 relation

Fig. 25 shows the effects of the weight W of powder filled into die on the P_U-e (porosity) relations. From these P_U-e relations, we can obtain the relation between e and W at any constant upper punch pressure. Results are shown in Fig. 26.

Fig. 26 shows that we can assume the e-W relations to be linear: this assumption is different from that in the previous paper.[15] The porosities at the zero weight, e_{ext}, obtained by extrapolation method are shown in Fig. 25. Identifying P_U as σ_1 and calculating $\bar{h}$ according to Eq. (74):

$$\bar{h} = \frac{1-e_{ext,0}}{1-e_{ext}} \tag{74}$$

we can determine the $\bar{h}$- σ_1 relation. The results are shown in Fig. 27, where the dotted line corresponds to the zero porosity. In Eq. (74), $e_{ext,0}$ is the value of e_{ext} when $\sigma_1=0$.

4. The Results of Numerical Calculations

The fundamental theory, the models of numerical calculations and the mechanical properties of potassium chloride powder have already been described. In practice, if we were to carry out the calculations, for example, in which (r_W, 0) and (r_W, h) were regarded as singular points or in which the velocity dependences of the coefficients of wall friction and internal friction and the $\bar{h}$- σ_1 relation were introduced, the calculations on computors would become very time-consuming. Besides, we have not yet given sufficient considerations to the stability of models and the convergence of solution in such the complicated calculations. Hence, the calculations were carried out on the base of assumptions for simplication.

4.1 The Pressure-transmission-ratio (P_L/P_U)——We reported in the previous paper[22] that the change in P_L/P_U accompanying an increase in P_U had the interesting patterns in the various powders. Hence, we tried to calculate P_L/P_U numerically.

The calculations of P_L/P_U were carried out under the following assumptions:

(1) The points (r_W, 0) and (r_W, h) are not singular.

(2) The arbitrary constants in Eq. (41) are as follows:

$$a_i = 0 \quad (i=3, 4, 5)$$
$$b_j = 0 \quad (j=4, 5, 6)$$

(3) The thickness h of the bed of powder takes the value obtained by numerically solving Eq. (75) for h.

$$W = \rho\int_0^h \int_0^{2\pi}\int_0^{r_W}(1-e_{ext})r\,dr\,d\theta\,dz \tag{75}$$

where ρ is the true density of potassium chloride powder equal to 1.988.

22) J. Okada and Y. Fukumori, *Chem. Pharm. Bull.* (Tokyo), **23**, 326 (1975).

The results of calculations are shown in Fig. 28 with $h/(2\,r_W)$ as abscissa against $\log(P_L/P_U)$ as ordinate. It is seen that the pressure-transmission-ratio takes the maximum value on the way of compression. In the case of 400 mesh, although the values at $P_U=50$ kg/cm^2 are on the straight line shown in Fig. 28, those at $P_U=900$ are on the curved line. Further, it is found that the wall friction have the remarkable effect on P_L/P_U.

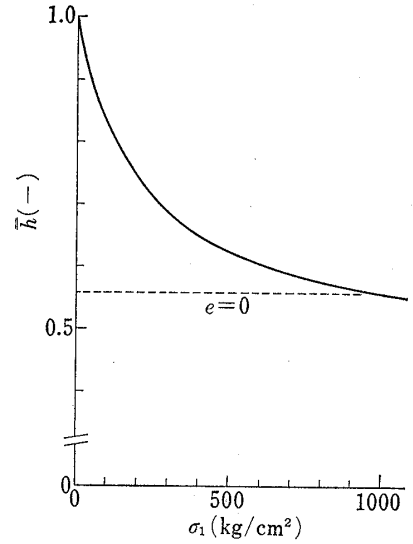

Fig. 27. Relation between $\bar{h}$ and σ_1

TABLE I. Calculated Values of the Constants in Eqs. (43) when $P_U=2$

a_1	1.984105
a_2	0.0
a_3	−0.583780
a_4	1.506932
a_5	−0.884962
b_1	0.0
b_2	−0.385488
b_3	4.681024
b_4	−11.661135
b_5	11.694262
b_6	−4.138283

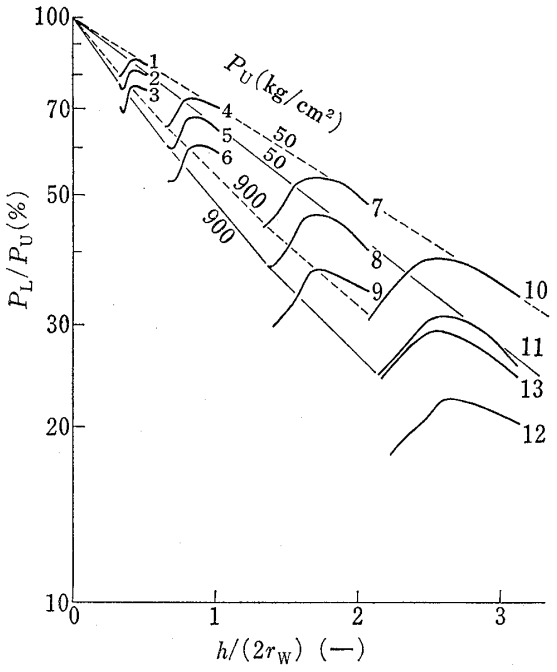

Fig. 28. Results of Calculations of P_L/P_U

1, 4, 7, 10: 400 mesh, μ_k.
(----: drawn through the values at $P_U=50$, 900)
2, 5, 8, 11: 400 mesh, μ_{s0}.
(——: drawn through the values at $P_U=50$, 900)
3, 6, 9, 12: 180 mesh, μ_{s0}.
13: 180 mesh, μ_k.
1, 2, 3: corresponding to the case where $(W, 2r_W)=(0.25$ g, 8.02 mm), (3.918 g, 20.11 mm) and so on.

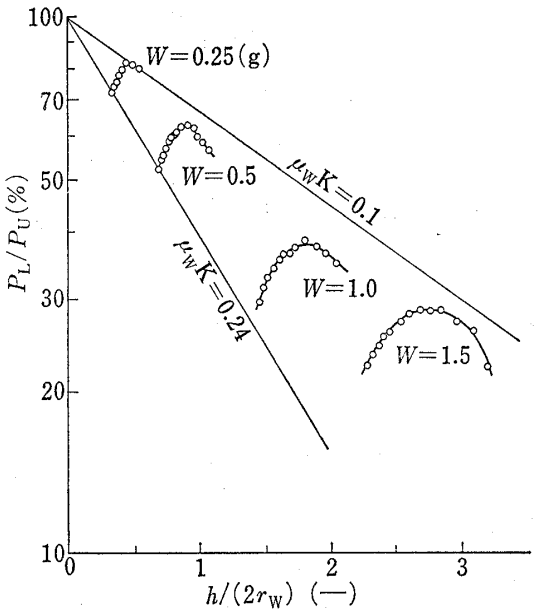

Fig. 29. Data of P_L/P_U Plotted according to the Janssen's Equation: $\ln(P_L/P_U)=-4\,\mu_W K(h/(2r_W))$ where K is Rankine's Constant

Rate of displacement of upper punch (mm/sec): 0.332.
Inside diameter of die $2r_W$ (mm): 8.02.

Data reported in the previous paper[22] are shown in Fig. 29. All the plots exist between the two lines which correspond to $\mu_W K=0.1$ and 0.24. However, it is difficult to compare the results of calculations by our model with the experimental data in detail, because in our calculations the effects of the velocity of sliding and the rate of displacement of upper punch on μ_W and the $\bar{h}$- σ_1 relation, respectively, *etc.*, are not considered. If described about μ_W, μ_W is generally affected by the velocity of sliding, which takes the values between zero at (r_W, h) and the rate of displacement of upper punch at (r_W, 0) in practice.

TABLE II. The Displacements of the Nodes on the Lower Punch and the Square of Deviation

k	r	$du_r \times 10^3$	du_z	$S_k \times 10^7$
1	0	0.0	−0.11758	4.1546
—	1	0.3792	−0.11771	—
2	2	0.5837	−0.11804	3.7575
—	3	0.5234	−0.11839	—
3	4	0.2857	−0.11858	2.0865
—	5	0.1220	−0.11854	—
4	6	0.1983	−0.11833	0.4978
—	7	0.4386	−0.11811	—
5	8	0.5701	−0.11804	3.5907
—	9	0.3119	−0.11820	—
6	10	0.0	−0.11896	5.4110

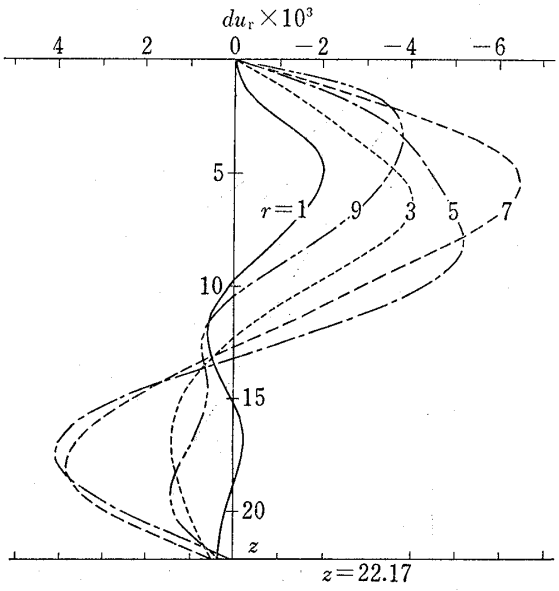

Fig. 30. Calculated Values of du_r

$z=22.17$: the measured thickness of the bed of powder under $P_U=0$.
—r=1—: du_r of the nodes whose r-coordinate is unity and so on.

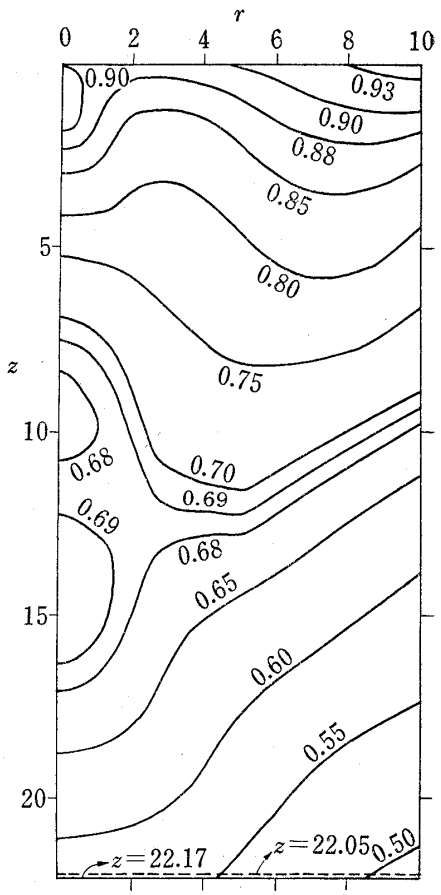

Fig. 31. Calculated Distribution of σ_Y (kg/cm^2)

$z=22.17$: the surface of lower punch at $P_U=0$.
$z=22.05$: the surface of lower punch at $P_U=2$.

4.2. The Distribution of Stress——In this section, the results of calculations in the case that any singular points are neither in the bed of powder nor on the boundary will be described. Calculations were carried out only in the case that P_U changes from zero to 2 kg/cm^2. The wall yield locus obtained from μ_k (180 mesh) was used.

For the unknown stress field where $P_U=0$, the following assumptions were set up:

(1) σ_Y is zero everywhere in the bed of powder.

(2) φ takes the same value as that when $P_U=2$ everywhere in the bed of powder.

The calculated values of the constants in Eq. (41) and the displacements of nodes on the lower punch are shown in Table I and II, respectively.

Fig. 30 and 31 show du_r and the distribution of σ_Y, respectively. In Fig. 31, it is interesting that the region where σ_Y takes the lower value than that in the neighbourhood and the region where σ_Y takes the higher value appear, though they have already been observed experimentally.[2,3] Although such regions appeared about the point (0, 3.5 r_W) in the case where calculations were carried out at $P_U=500$ under the assumptions in section (4.1), they appear about the middle of the bed when the displacements must satisfy the boundary conditions (51)—(53).

Acknowledgement The authors would like to express their thanks to Miss Yuko Tasaka, Mr. Masanobu Hiramatsu, Mr. Masamichi Kishishita, Mrs. Fumiko Sugihara and Miss Yoshiko Hirai for their helpful *co*-operations. The calculations were carried out on a FACOM 230-75 computors at the Data Processing Center of Kyoto University. Thanks are due to the staff of that center.